Environ. Sci. Technol. **2008,** *42,* 3459–3464

Mechanism of C_{60} Photoreactivity in Water: Fate of Triplet State and Radical Anion and Production of Reactive Oxygen Species

JAESANG LEE,[‡] YOKO YAMAKOSHI,[†] JOSEPH B. HUGHES,[‡] AND JAE-HONG KIM*,[‡]

Department of Radiology, University of Pennsylvania, Philadelphia, Pennsylvania 19104, and School of Civil and Environmental Engineering, Georgia Institute of Technology, Atlanta, Georgia 30332-0373

Received November 19, 2007. Revised manuscript received January 15, 2008. Accepted February 06, 2008.

The mechanism involved with (1) energy and electron transfer by C_{60} in the aqueous phase during UV irradiation and (2) subsequent production of reactive oxygen species (ROS) such as singlet oxygen and superoxide radical anion was investigated. Electron paramagnetic resonance (EPR) study showed that C_{60} embedded in micelles of nonionic surfactant (Triton X 100) or anionic surfactant (sodium dodecylbenzenesulfonate) produced ROS, but aggregated C_{60} did not, consistent with our earlier findings made using indicator chemicals. Nanosecond and femtosecond laser flash photolysis showed that the aggregation of C_{60} significantly accelerates the decay of excited triplet state C_{60}, which is a key intermediate for energy and electron transfer, thus blocking the pathway for ROS production. This finding suggests that C_{60} clusters will not contribute to oxidative damage or redox reactions in natural environment and biological systems in the same way molecular C_{60} in organic phase reportedly does. In contrast, C_{60} embedded in surfactant micelles produces ROS and the evidence is presented for the formation of C_{60} radical anion as an intermediate.

Introduction

Understanding photochemical properties of C_{60} is critical to accurately assess C_{60}'s ecotoxicological impact upon unwanted release to the natural environment (*1–3*). When irradiated with UV light (*4*), C_{60} is photochemically excited to singlet state ($^1C_{60}$*), which subsequently converts to triplet state ($^3C_{60}$*) through intersystem crossing (*5–7*). The excess energy in $^3C_{60}$* is efficiently transferred to oxygen present in the same media as C_{60} returns to ground state (*6, 7*), producing singlet oxygen, $^1O_2$ (*5, 8–11*). In the presence of an electron donor with an adequate redox potential, $^3C_{60}$* can be reductively converted to C_{60} radical anion ($C_{60}^{\bullet-}$) (*9–12*), which further transfers an electron to oxygen, producing superoxide radical anion, $O_2^{\bullet-}$ (*9–11*). Such electron transfer mechanisms are thermodynamically much more favorable with $^3C_{60}$* than ground-state C_{60} ($E^0(^3C_{60}^*/^3C_{60}^{\bullet-}) = +1.1\ V_{NHE}$ vs $E^0(^1C_{60}/^1C_{60}^{\bullet-}) = -0.2\ V_{NHE}$ (*13*)). Therefore, it is possible that photoexcited C_{60} can be involved in various redox reactions as either an electron acceptor or electron shuttle. These properties, particularly C_{60}'s ability to produce reactive oxygen species (ROS) such as $^1O_2$ and $O^{2\bullet-}$, have been proposed as the mechanism of observed toxicological effects of C_{60} (*2, 14, 15*).

However, C_{60} does not always exhibit the above intrinsic molecular properties. Our past study (*9*) suggested that when C_{60} formed stable aggregates in water, $^1O_2$ and $O_2^{\bullet-}$ production was not measurable by wet chemical methods. Note that the aggregate forms of C_{60} can be produced via different preparation methods including (1) solvent exchange using polar organic solvent such as tetrahydrofuran (*16–18*), (2) contacting organic solvent containing C_{60} with water and applying ultrasound (*9, 19, 20*), or (3) mixing dry C_{60} with water for an extended period (*16*), among others. These aggregate forms of C_{60} have raised an environmental issue as the new form of C_{60} that can potentially contaminate natural waterways (*1–3, 18, 21, 22*). In contrast, when C_{60} was associated with encapsulating agents such as surfactant or polymer, C_{60} retained its intrinsic photochemical reactivity (*9–11, 23*). These findings are significant as they suggest that C_{60} released to the aqueous environment as aggregates may not be directly involved with ROS-induced toxicological effects reported in the past, as long as they are not physically or chemically modified as they enter a biological system.

The present study provides key experimental evidence to elucidate the mechanisms of how energy and electron transfer by C_{60} are affected by the dispersion status of C_{60} in the aqueous phase. We hypothesized in our past study (*9*) that when C_{60} forms aggregate, the reaction intermediate, i.e., photoexcited triplet C_{60} ($^3C_{60}$*), is quenched by surrounding ground-state C_{60} (self-quenching) and another triplet C_{60} (triplet–triplet annihilation), resulting in loss of intrinsic photochemical reactivity. This hypothesis is tested herein by measuring the lifetime of key intermediate species for energy transfer ($^3C_{60}$*) and electron transfer ($C_{60}^{\bullet-}$) using nanosecond and femtosecond laser flash photolysis. In particular, detection of $C_{60}^{\bullet-}$ in the presence of strong electron donor (i.e., triethylamine (TEA)) would indicate that a direct involvement of C_{60} as an electron acceptor or mediator in various redox reactions might be possible in the natural environment and biological systems. We examine several representative water stable C_{60} samples, including C_{60} aggregates prepared according to previously established methods (*9, 19*) and C_{60} associated with two different types of surfactants, Triton X 100 (TX 100, nonionic) and sodium dodecylbenzenesulfonate (SDBS, anionic), that were applied either below or above critical micelle concentration (c.m.c.). In our past study (*9*), ROS productions were indirectly measured using furfuryl alcohol and nitro blue tetrazolium as an indicator for $^1O_2$ and $O_2^{\bullet-}$ respectively. In this study, we apply an electron paramagnetic resonance (EPR) spin trapping technique which is more commonly used to detect radical species.

Experimental Section

Materials. Chemicals used as received in this study include: C_{60} (99.9%, sublimed, MER Corp.), SDBS (Aldrich, c.m.c. = ca. 1.7 g/L), TX 100 (Sigma-Aldrich, c.m.c. = ca. 0.16 g/L), TEA (Aldrich), toluene (Fisher Scientific), 2,2,6,6-tetramethyl-4-piperidone (4-oxo-TEMP, Tokyo Chemical Industries), 5,5-dimethyl-1-pyrroline-*N*-oxide (DMPO, DOJINDO Laboratories), $FeSO_4$ (Sigma-Aldrich), and diethylenetriaminepentaacetic acid (DETAPAC, Sigma-Aldrich). Ultrapure water (resistance >18.2 MΩ) produced by a Milli-Q water purification system (Millipore, Billerica, MA) was used for the preparation of all solutions.

* Corresponding author e-mail: jaehong.kim@ce.gatech.edu; phone: (404) 894-2216; fax: (404) 385-7087.
† University of Pennsylvania.
‡ Georgia Institute of Technology.

10.1021/es702905g CCC: $40.75 © 2008 American Chemical Society
Published on Web 04/01/2008

Preparation of Aqueous Stable C_{60}. Ultrasound (50/60 Hz, 125 W) was applied to a heterogeneous mixture of 10 mL of toluene containing 5 mg of C_{60} and 90 mL of ultrapure water in a sealed bottle for 24 h using an ultrasonicator (model 8845-40, Cole-Parmer). The ultrasound was further applied to the mixture open to atmosphere for an additional 24 h at 60 °C to evaporate toluene. The solution was then filtered through a 0.45-μm PTFE filter (Millipore Corp.). The aqueous suspension of aggregate form of C_{60} prepared according to this specific method is herein referred to as son/C_{60}. C_{60} associated with surfactants was prepared following the same procedure except that the ultrapure water contained surfactant. These are referred to in this study as C_{60}/TX 100 or C_{60}/SDBS.

EPR Analysis. EPR analyses were performed using a Bruker EMX spectrometer under the following conditions: temperature = 298 K, microwave frequency = 9.8 GHz, microwave power = 16 mW, field modulation = 0.1 mT at 100 kHz, and scan time = 89.3 s.

(1) *$^1O_2$ Detection.* Production of $^1O_2$ was monitored using 4-oxo-TEMP as a spin-trapping reagent (*11*). Experimental solution with the target C_{60} concentration of 5 mg/L was prepared by mixing 1 M 4-oxo-TEMP (20 μL), 12.5 mg/L C_{60} stock suspension (100 μL), 250 mM phosphate buffer at pH 7.0 (50 μL), and ultrapure water (80 μL). The solution was placed in a cylindrical quartz cell and UV light (350–400 nm) was irradiated using six 4-W black light bulbs (BLB, Philips TL4W). After the light irradiation for 3–20 min (i.e., not beyond 30 min to avoid the excessive degradation of 4-oxo-TEMP), the test cell was quickly subjected to EPR measurement. When $^1O_2$ was produced, 4-oxo-TEMP was oxidized by $^1O_2$ to produce 4-oxo-2,2,6,6-tetramethyl-1-piperdinyloxy radical (4-oxo-TEMPO). The EPR signals for 4-oxo-TEMPO therefore indicated the formation of $^1O_2$.

(2) *$O_2^{\bullet-}$ Detection.* The generation of $O_2^{\bullet-}$ was indirectly measured by converting $O_2^{\bullet-}$ to $^\bullet$OH *in situ* and monitoring $^\bullet$OH, since $^\bullet$OH can be more sensitively detected by the EPR spin-trapping technique (*11*). Fe(II)−DETAPAC complex was used to reduce $O_2^{\bullet-}$ to $^\bullet$OH [k(Fe(II)−DETAPAC + $O_2^{\bullet-}$) = (2 ± 0.5) × 10^7 $M^{-1}s^{-1}$ (*24*)]. DMPO was utilized as a spin-trapping agent for $^\bullet$OH and TEA was used as an electron donor. The reaction mixture was prepared by mixing DMPO (20 μL), 5 mM Fe(II)−DETAPAC in 250 mM phosphate buffer (50 μL), 12.5 mg/L C_{60} stock suspension (100 μL), 100 mM TEA (25 μL), and distilled water (55 μL). The photochemical reaction was performed following the same procedure described above for $^1O_2$ and EPR signals of DMPO-OH adduct were monitored.

Laser Flash Photolysis. (1) *Decay Kinetics of $^3C_{60}$*.* Both nanosecond and femtosecond laser flash photolysis experiments were carried out to trace the decay kinetics of $^3C_{60}$* in different aqueous C_{60} samples. The experimental solution contained 5 mg/L of C_{60} and was buffered at pH 7. To inhibit the pathway for energy transfer from $^3C_{60}$* to oxygen, solution (3 mL) was placed in a rectangular cell, bubbled with argon gas for 30 min, and sealed from the atmosphere. For nanosecond experiments, a 355 nm laser pulse (10 mJ, pulse width = 6 ns) from a Quanta Ray Nd:YAG laser system was used as an excitation source and a xenon lamp was used as a monitoring source. Instantaneous formation of $^3C_{60}$* after laser pulse and subsequent decay were monitored at 740 nm (*6*). For the C_{60} samples with $^3C_{60}$* having short life times (less than a nanosecond), femtosecond laser flash photolysis experiments were performed using a Clark-MXR 2010 laser. A 387 nm laser pulse (attenuated to 5 μJ, pulse width = 150 fs) obtained by introducing a second harmonic generator to the path of the laser beam from a Clark laser system was used as an excitation source. Time-resolved spectra in the wavelength region from 425 to 800 nm were obtained using a Helios transient absorption spectrometer (Ultrafast System).

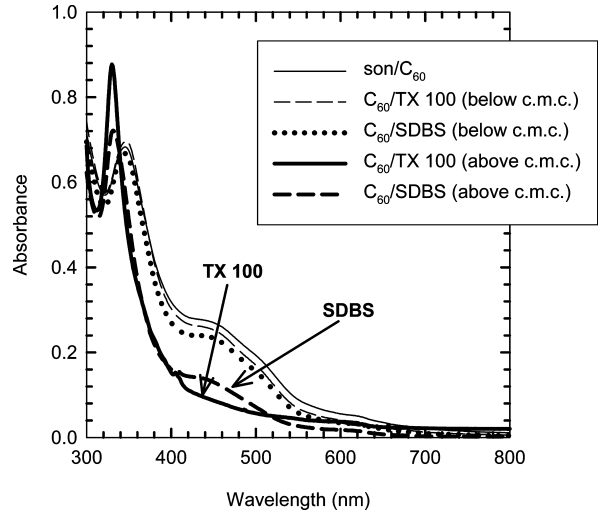

FIGURE 1. UV–visible absorption spectra of son/C_{60} and C_{60} colloids associated with TX 100 and SDBS applied below and above c.m.c. ([TX 100 (below c.m.c.)]$_0$ = 0.1 g/L; [TX 100 (above c.m.c.)]$_0$ = 50 g/L; [SDBS (below c.m.c.)]$_0$ = 0.2 g/L; [SDBS (above c.m.c.)]$_0$ = 20 g/L; [phosphate]$_0$ = 50 mM; pH$_i$ = 7).

Decay kinetics for $^3C_{60}$* was obtained from the time-resolved data using absorbance at 740 nm.

(2) *Decay Kinetics of $C_{60}^{\bullet-}$.* Transient formation of $C_{60}^{\bullet-}$ through one-electron transfer from TEA under UV irradiation and subsequent decay were monitored using a nanosecond laser flash photolysis which was conducted with 308 nm laser pulses from Lambda Physik excimer laser system (10 mJ, pulse width 10 ns). The experiments were carried out under the anoxic condition (by Argon purging) so that energy transfer from $^3C_{60}$* to O_2 and electron transfer from $C_{60}^{\bullet-}$ to O_2 are both blocked. Concentration of $C_{60}^{\bullet-}$ was monitored by recording the transient absorption at 1050 nm in Near-IR region (*25*).

Results and Discussion

Photochemical Production of Singlet Oxygen. UV–vis spectra of son/C_{60} and C_{60} associated with TX 100 or SDBS (Figure 1), suggested that son/C_{60} and C_{60} associated with TX 100 and SDBS applied below c.m.c. formed aggregates, as evidenced by a rather strong broad band absorption in the wavelength region from 400 to 500 nm (*17, 18*). C_{60} aggregates in these samples are ca. 50−200 nm in size according to dynamic light scattering (DLS) measurements by our past study as well as others (*9, 19, 20*). In contrast, when surfactants were applied above c.m.c. aggregation was considerably reduced, as evidenced by lower absorbance in the visible regions and less red-shifted specific peaks compared to UV–vis spectrum of son/C_{60} (*17, 18, 26*). It is suspected that C_{60} associated with SDBS applied above c.m.c. might have a minor degree of aggregation, while no definite evidence was possible. Note that DLS measurements of these samples approached the instrument detection limit (ca. 5 nm). Microscopic imaging using transmission electron microscope (TEM) was not possible as excessive surfactant deposited on the carbon grid prevented clear images.

Figures 2a and 2b show that the specific EPR signals for 4-oxo-TEMPO (i.e., $^1O_2$ adduct with 4-oxo-TEMP) were produced when the UV light was irradiated to the C_{60} associated with TX 100 and SDBS (above c.m.c.). The peak height increased as UV irradiation time was increased. In marked contrast, C_{60} associated with TX 100 and SDBS (below c.m.c.) and son/C_{60} did not produce any specific EPR signal for 4-oxo-TEMPO (Figures 2c–2e). These C_{60} present as aggregate form exhibited strong broad band visible light absorption. These EPR observations are consistent with our

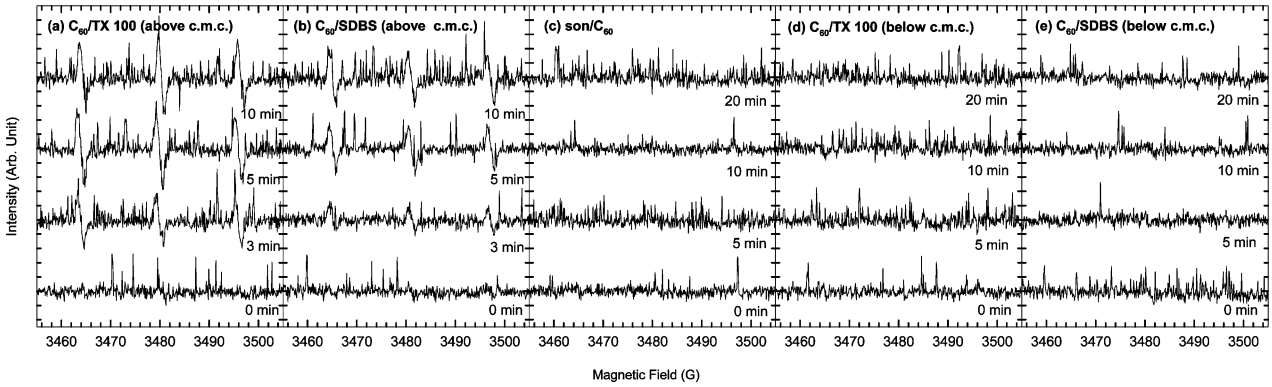

FIGURE 2. EPR spectra of 4-oxo-TEMP adduct with $^1O_2$ produced in the UV–vis illuminated suspension of (a) C_{60}/TX 100 (above c.m.c.), (b) C_{60}/SDBS (above c.m.c.), (c) son/C_{60}, (d) C_{60}/TX 100 (below c.m.c.), and (e) C_{60}/SDBS (below c.m.c.) ([son/C_{60}]$_0$ = [C_{60}/TX 100]$_0$ = [C_{60}/SDBS]$_0$ = 5 mg/L; [4-oxo-TEMP]$_0$ = 80 mM; [phosphate]$_0$ = 50 mM; pH$_i$ = 7).

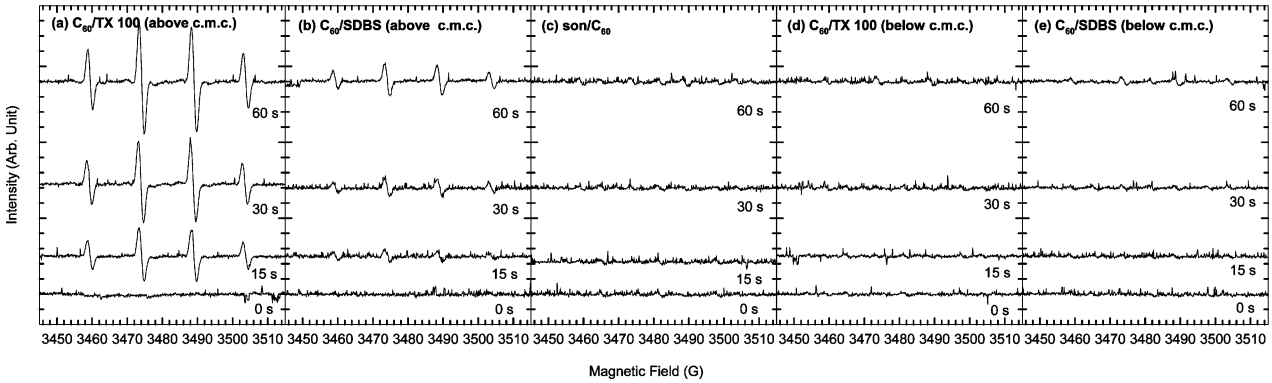

FIGURE 3. EPR spectra of DMPO adduct with OH radical produced in the UV–vis illuminated suspension of (a) C_{60}/TX 100 (above c.m.c.), (b) C_{60}/SDBS (above c.m.c.), (c) son/C_{60}, (d) C_{60}/TX 100 (below c.m.c.), and (e) C_{60}/SDBS (below c.m.c.) with Fe(II)−DETAPAC and TEA as an electron donor ([son/C_{60}]$_0$ = [C_{60}/TX 100]$_0$ = [C_{60}/SDBS]$_0$ = 5 mg/L; [DMPO]$_0$ = 0.72 M; [Fe(II)-DETAPAC]$_0$ = 5 mM; [TEA]$_0$ = 10 mM; [phosphate]$_0$ = 50 mM; pH$_i$ = 7).

past conclusion driven from wet chemical analyses that C_{60} with greater degree of aggregation is less photochemically active with respect to $^1O_2$ production (i.e., inefficient transfer of energy from $^3C_{60}$* to oxygen) (*9*). It is also noteworthy that C_{60} encapsulated in the micelles of TX 100 produced stronger EPR signals than that with SDBS. TX 100 prohibited C_{60} aggregation more effectively than SDBS, resulting in lower visible light absorption, more $^1O_2$ production, and stronger 4-oxo-TEMPO signals.

Photochemical Production of Superoxide Radical Anion. The EPR signals of DMPO−OOH adducts that are produced from a slow reaction between DMPO and $O_2^{\bullet-}$ [k(DMPO + $O_2^{\bullet-}$) = 10 $M^{-1}s^{-1}$ (*24*)] were short-lived and exhibited complicated patterns (data not shown). Although the appearance of signals indicated the generation of $O_2^{\bullet-}$ in some samples (i.e., C_{60} associated with TX 100 and SDBS applied above c.m.c.), it was difficult to draw a definite conclusion based on these signals. As an alternative approach, $O_2^{\bullet-}$ was converted to $^{\bullet}$OH *in situ* by ferrous complex (Fe(II)−DETAPAC), and DMPO−OH adduct that results from the reaction between DMPO and $^{\bullet}$OH was examined. A control test was performed with Fe(II)−DETAPAC in the absence of C_{60}, and no DMPO−OH signals were detected during UV irradiation, suggesting that the iron catalyst would not contribute to formation of both OH radical and $O_2^{\bullet-}$.

As shown in Figure 3, C_{60} associated with TX 100 and SDBS applied above c.m.c. produced specific signals for DMPO−OH adducts of which strengths were dependent on UV irradiation time. In contrast, son/C_{60} and C_{60} associated with TX 100 and SDBS applied below c.m.c. did not. This result suggests that electron transfer from TEA to oxygen is effectively mediated by C_{60} embedded in micelle assembly which inhibits C_{60} aggregation. Accordingly, C_{60} encapsulated with TX 100 showed greater signal strength than SDBS, as TX 100 was more efficient for inhibiting C_{60} clustering in the aqueous phase. These EPR results are consistent with our past conclusion, similar to $^1O_2$, that production of $O_2^{\bullet-}$ is also dependent on the degree of C_{60} clustering, i.e., the greater the degree of aggregation, the less $O_2^{\bullet-}$ production (*9*).

Decay Kinetics of $^3C_{60}$*. The above phenomena might result as $^3C_{60}$*, a critical transient intermediate for both energy transfer (i.e., $^1O_2$ generation) and electron transfer (i.e., $O_2^{\bullet-}$ production), is rapidly lost when C_{60} forms a cluster. When $^3C_{60}$* is in direct contact with other C_{60} molecules, energy can be rapidly dissipated through a self-quenching mechanism (i.e., energy transfer to surrounding ground-state C_{60}) and triplet–triplet annihilation (i.e., energy transfer to another $^3C_{60}$*). A time-resolved laser flash photolysis was used to trace $^3C_{60}$* under anoxic, argon saturated condition (where $^3C_{60}$* decay pathway due to energy transfer to oxygen can be excluded) to verify the above hypothesis (*6*). Specifically, the absorption of $^3C_{60}$* at 740 was measured.

Figure 4 shows that $^3C_{60}$* decayed over the time scale of a few hundred microseconds when C_{60} was embedded in TX 100 and SDBS micelles. The rate of anoxic depletion of $^3C_{60}$* observed herein was comparable to that of $^3C_{60}$* molecularly dissolved in organic phase or monomeric analogue of C_{60} derivative in water (*27*). C_{60} embedded in TX 100 micelles is most likely to be molecularly dispersed within the micelle core (i.e., no specific visible range absorption, Figure 1), and therefore the decay of triplet state by the self-quenching and triplet–triplet annihilation proceeds most slowly, among all C_{60} samples. C_{60} in SDBS may not be monomeric but have some level of aggregation (i.e., some visible absorption, Figure 1), while no direct experimental evidence is currently available as mentioned above. Consequently, the anoxic decay kinetics

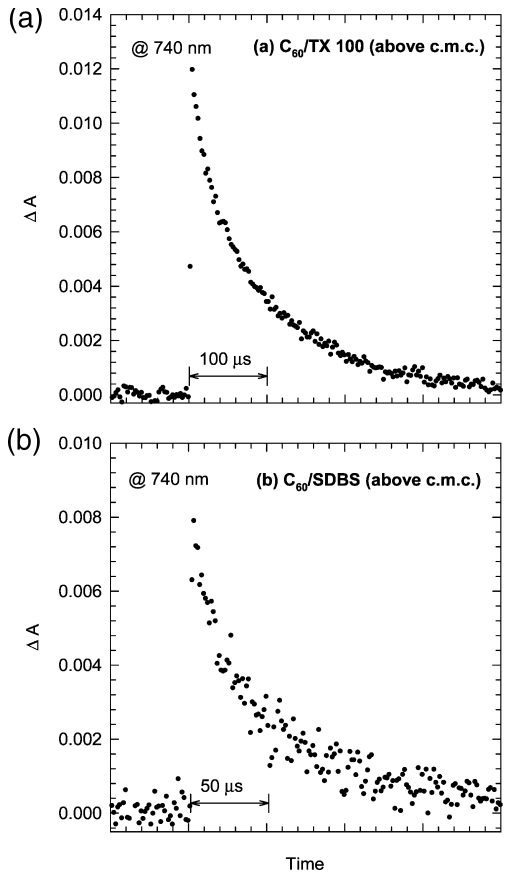

FIGURE 4. Absorption time profile of $^3C_{60}$* recorded at 740 nm in aqueous suspension of (a) C_{60}/TX 100 (above c.m.c.) and (b) C_{60}/SDBS (above c.m.c.) ($[C_{60}/TX\ 100]_0 = [C_{60}/SDBS]_0 = 5$ mg/L; $[phosphate]_0 = 50$ mM; $pH_i = 7$; Ar-saturated condition).

of triplet state of this C_{60} is, albeit considerably retarded as well, faster than triplet depletion rate of C_{60}/TX 100 (above c.m.c.). The laser flash photolysis results suggest that the lifetime of $^3C_{60}$* in these C_{60} colloids is sufficiently long such that energy transfer from $^3C_{60}$* to O_2 competes other anoxic quenching pathways. As a result, $^1O_2$ production was observed in EPR analysis. This spectral difference is also well reflected by the laser flash photolysis and EPR measurements. The initial absorption difference, ΔA, obtained immediately after laser-excitation was much higher for C_{60} in TX 100 than SDBS (Figure 4), which, combined with much longer lifetime of $^3C_{60}$* of C_{60}/TX 100 (above c.m.c.), might imply more efficient formation of $^3C_{60}$* when C_{60} is molecularly dispersed. Accordingly, the EPR signals were greater with C_{60} in TX 100 indicating greater level of both $^1O_2$ and $O_2^{\bullet-}$ production (Figures 2 and 3).

However, no distinguishable peaks were observed for C_{60} clusters (i.e., son/C_{60} and C_{60} associated with TX 100 and SDBS applied below c.m.c.) using the nanosecond laser flash photolysis. Lack of peaks could have resulted if the time scale of decay is smaller than the time scale of measurement. Therefore, the measurement time scale was reduced and additional experiments were performed using femtosecond laser flash photolysis. Figure 5 shows the absorption spectra recorded during initial 4 ps after the excitation by pulse laser irradiation. The peak centered around 740 nm, which indicated $^3C_{60}$* increased over the first 2 ps, and rapidly disappeared within the next 2 ps.

Compared to C_{60} in TX 100 and SDBS micelles, the decay kinetics of triplet state was significantly accelerated when C_{60} formed aggregates. The half-lives of $^3C_{60}$* in TX 100 and SDBS micelles were ca. 70 and 30 μs, respectively, while those of $^3C_{60}$* in clusters were less than 1 ps. This result confirms the hypothesis that energy transfer process and $^1O_2$ production pathway are fundamentally blocked due to C_{60} aggregation and consequent rapid loss of critical intermediate during energy transfer process. As $^3C_{60}$* becomes short-lived and less available, electron transfer from electron donor to $^3C_{60}$* is also limited and consequently $O_2^{\bullet-}$ production pathway is prohibited.

Decay Kinetics of Radical Anion of C_{60} Colloid. C_{60} radical anion ($C_{60}^{\bullet-}$) is a critical intermediate for production of $O_2^{\bullet-}$ and for any other redox reactions involving electron abstraction or electron transfer mediation by C_{60}. Using a laser flash photolysis, transient formation and decay of $C_{60}^{\bullet-}$ was monitored. An absorption at 1050 nm was recorded as $C_{60}^{\bullet-}$ exhibits strong absorption in IR region (*25*).

Figure 6 shows that $C_{60}^{\bullet-}$ formed when a solution containing C_{60} in TX 100 micelle and TEA was irradiated with a pulse laser at 308 nm and decayed over approximately 0.3 ms. The kinetics of formation and decay were comparable to $^3C_{60}$* (Figure 4) suggesting that electron transfer from the electron donor to $^3C_{60}$* occurred at a faster rate than the time scale of experiments. In contrast, no measurable peak for $C_{60}^{\bullet-}$ was detected for clustered C_{60} (son/C_{60} and C_{60} with surfactants below c.m.c.) (results not shown). This result was consistent with the observations made for $^3C_{60}$* as well as $O_2^{\bullet-}$ production recorded by EPR and spectral properties.

The results presented in this study help understand the environmental impact of C_{60} aggregate, a form of C_{60} that

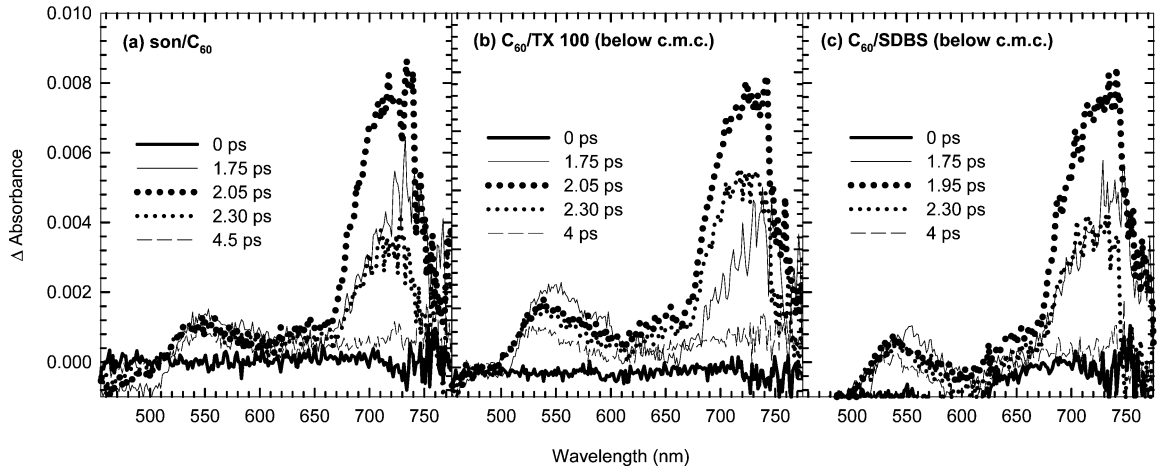

FIGURE 5. Time-resolved differences absorption spectra of triplet state of (a) aqueous son/C_{60}, (b) C_{60}/TX 100 (below c.m.c.), and (c) C_{60}/SDBS (below c.m.c.) colloid ($[son/C_{60}]_0 = [C_{60}/TX\ 100]_0 = [C_{60}/SDBS]_0 = 5$ mg/L; $[phosphate]_0 = 50$ mM; $pH_i = 7$).

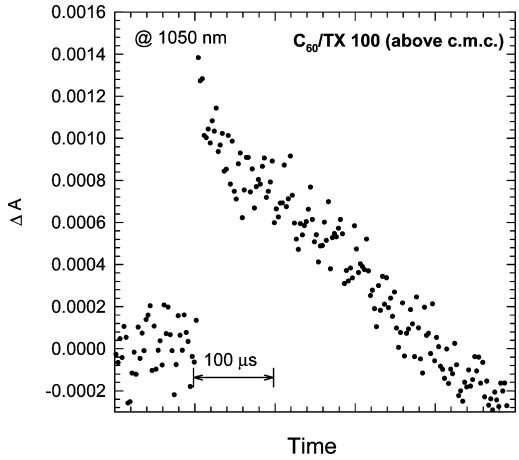

FIGURE 6. Absorption time profile of $C_{60}^{\bullet-}$ recorded at 1050 nm in aqueous suspension of C_{60}/TX 100 (above c.m.c.) ([C_{60}/TX 100]$_0$ = 5 mg/L; [TEA]$_0$ = 10 mM; [phosphate]$_0$ = 50 mM; pH$_i$ = 7; Ar-saturated condition).

has received a widespread concern as a possible pollutant form of C_{60} in natural waterways. The EPR measurement of ROS presented in this study confirms that C_{60} clustering results in loss of C_{60}'s intrinsic photoreactivity. Laser flash photolysis suggests that this loss results as the lifetime of key intermediate species is drastically reduced when C_{60} forms aggregate. Therefore, aggregate C_{60} themselves will not be responsible for oxidative damage by photochemical ROS production in the natural environment and biological systems, contrary to some suggestions made in the past (*28–30*). In contrast, C_{60} might participate in ROS production as it is embedded in surfactant micelles or other natural encapsulating agents which prevent C_{60} aggregation.

It is also noteworthy that $C_{60}^{\bullet-}$ did not form when C_{60} was aggregated even under relatively favorable conditions for reduction (i.e., in the presence of a strong electron donor and under UV irradiation). C_{60} reduction is thermodynamically favorable when the reduction potential of triplet state, molecular C_{60} is considered ($E^0(^3C_{60}^*/^3C_{60}^{\bullet-}) = +1.1$). Therefore, the electron transfer process is kinetically limited when C_{60} forms aggregates and the reaction intermediate is quenched. This suggests that aggregate C_{60} in most natural and biological environments will not directly participate in redox reactions (i.e., as an electron acceptor or electron mediator), while a definite conclusion cannot be made at current stage. Since changes in dispersion status as C_{60} enters the biological system are suspected, further study is necessary to trace the photochemical properties of C_{60} that interact with biomolecules.

Acknowledgments

This work was funded by the United States Environmental Protection Agency (USEPA) STAR Grant D832526. We thank Mark Lingwood at Department of Chemistry and Biochemistry, University of California, Santa Barbara for assistance with EPR measurements, Dr. Prashant Kamat, Dr. Matsunaga Yoichiro, and Kevin Tvrdy at Radiation Laboratory, University of Notre Dame, for fruitful discussions and assistance with laser flash photolysis experiments.

Literature Cited

(1) Colvin, V. L. The potential environmental impact of engineered nanomaterials. *Nat. Biotechnol.* **2003**, *21*, 1166–1170.
(2) Sayes, C. M.; Fortner, J. D.; Guo, W.; Lyon, D.; Boyd, A. M.; Ausman, K. D.; Tao, Y. J.; Sitharaman, B.; Wilson, L. J.; Hughes, J. B.; West, J. L.; Colvin, V. L. The differential cytotoxicity of water-soluble fullerenes. *Nano Lett.* **2004**, *4*, 1881–1887.
(3) Wiesner, M. R.; Lowry, G. V.; Alvarez, P.; Dionysiou, D.; Biswas, P. Assessing the risks of manufactured nanomaterials. *Environ. Sci. Technol.* **2006**, *40*, 4336–4345.
(4) Lof, R. W.; van Veenendaal, M. A. K. B.; Jonkman, H. T.; Sawatzky, G. A. Band gap, excitons, and Coulomb interaction in solid C_{60}. *Phys. Rev. Lett.* **1992**, *68*, 3924–3927.
(5) Arbogast, J. W.; Darmanyan, A. P.; Foote, C. S.; Rubin, Y.; Diederich, F. N.; Alvarez, M. M.; Anz, S. J.; Whetten, R. L. Photophysical properties of C_{60}. *J. Phys. Chem.* **1991**, *95*, 11–12.
(6) Dimitrijevic, N. M.; Kamat, P. V. Triplet excited-state behavior of fullerenes - pulse-radiolysis and laser flash photolysis of C_{60} and C_{70} in benzene. *J. Phys. Chem.* **1992**, *96*, 4811–4814.
(7) Fraelich, M. R.; Weisman, R. B. Triplet-states of C_{60} and C_{70} in solution - Long intrinsic lifetimes and energy pooling. *J. Phys. Chem.* **1993**, *97*, 11145–11147.
(8) Jensen, A. W.; Daniels, C. Fullerene-coated beads as reusable catalysts. *J. Org. Chem.* **2003**, *68*, 207–210.
(9) Lee, J.; Fortner, J. D.; Hughes, J. B.; Kim, J. H. Photochemical production of reactive oxygen species by C_{60} in the aqueous phase during UV irradiation. *Environ. Sci. Technol.* **2007**, *41*, 2529–2535.
(10) Yamakoshi, Y.; Sueyoshi, S.; Fukuhara, K.; Miyata, N. OH and O_2^- generation in aqueous C_{60} and C_{70} solutions by photoirradiation: An EPR study. *J. Am. Chem. Soc.* **1998**, *120*, 12363–12364.
(11) Yamakoshi, Y.; Umezawa, N.; Ryu, A.; Arakane, K.; Miyata, N.; Goda, Y.; Masumizu, T.; Nagano, T. Active oxygen species generated from photoexcited fullerene (C_{60}) as potential medicines: O_2^- versus $^1O_2$. *J. Am. Chem. Soc.* **2003**, *125*, 12803–12809.
(12) Arbogast, J. W.; Foote, C. S.; Kao, M. Electron transfer to triplet C_{60}. *J. Am. Chem. Soc.* **1992**, *114*, 2277–2279.
(13) Kamat, P. V.; Haria, M.; Hotchandani, S. C_{60} cluster as an electron shuttle in a Ru(II)-polypyridyl sensitizer-based photochemical solar cell. *J. Phys. Chem. B* **2004**, *108*, 5166–5170.
(14) Dhawan, A.; Taurozzi, J. S.; Pandey, A. K.; Shan, W. Q.; Miller, S. M.; Hashsham, S. A.; Tarabara, V. V. Stable colloidal dispersions of C_{60} fullerenes in water: Evidence for genotoxicity. *Environ. Sci. Technol.* **2006**, *40*, 7394–7401.
(15) Isakovic, A.; Markovic, Z.; Todorovic-Markovic, B.; Nikolic, N.; Vranjes-Djuric, S.; Mirkovic, M.; Dramicanin, M.; Harhaji, L.; Raicevic, N.; Nikolic, Z.; Trajkovic, V. Distinct cytotoxic mechanisms of pristine versus hydroxylated fullerene. *Toxicol. Sci.* **2006**, *91*, 173–183.
(16) Brant, J.; Lecoanet, H.; Hotze, M.; Wiesner, M. Comparison of electrokinetic properties of colloidal fullerenes (nC_{60}) formed using two procedures. *Environ. Sci. Technol.* **2005**, *39*, 6343–6351.
(17) Deguchi, S.; Alargova, R. G.; Tsujii, K. Stable dispersions of fullerenes, C_{60} and C_{70}, in water. Preparation and characterization. *Langmuir* **2001**, *17*, 6013–6017.
(18) Fortner, J. D.; Lyon, D. Y.; Sayes, C. M.; Boyd, A. M.; Falkner, J. C.; Hotze, E. M.; Alemany, L. B.; Tao, Y. J.; Guo, W.; Ausman, K. D.; Colvin, V. L.; Hughes, J. B. C_{60} in water: Nanocrystal formation and microbial response. *Environ. Sci. Technol.* **2005**, *39*, 4307–4316.
(19) Andrievsky, G. V.; Kosevich, M. V.; Vovk, O. M.; Shelkovsky, V. S.; Vashchenko, L. A. On the production of an aqueous colloidal solution of fullerenes. *J. Chem. Soc., Chem. Commun.* **1995**, 1281–1282.
(20) Chen, K. L.; Elimelech, M. Aggregation and deposition kinetics of fullerene (C_{60}) nanoparticles. *Langmuir* **2006**, *22*, 10994–11001.
(21) Fang, J. S.; Lyon, D. Y.; Wiesner, M. R.; Dong, J. P.; Alvarez, P. J. J. Effect of a fullerene water suspension on bacterial phospholipids and membrane phase behavior. *Environ. Sci. Technol.* **2007**, *41*, 2636–2642.
(22) Lyon, D. Y.; Adams, L. K.; Falkner, J. C.; Alvarez, P. J. J. Antibacterial activity of fullerene water suspensions: Effects of preparation method and particle size. *Environ. Sci. Technol.* **2006**, *40*, 4360–4366.
(23) Beeby, A.; Eastoe, J.; Heenan, R. K. Solubilization of C_{60} in aqueous micellar solution. *J. Chem. Soc., Chem. Commun.* **1994**, 173–175.
(24) Bielski, B. H. J.; Cabelli, D. E.; Arudi, R. L.; Ross, A. B. Reactivity of HO_2/O_2^- radicals in aqueous solution. *J. Phys. Chem. Ref. Data* **1985**, *14*, 1041–1100.
(25) Nakanishi, I.; Fukuzumi, S.; Konishi, T.; Ohkubo, K.; Fujitsuka, M.; Ito, O.; Miyata, N. DNA cleavage via superoxide anion formed in photoinduced electron transfer from NADH to *r*-cyclodextrin-bicapped C_{60} in an oxygen-saturated aqueous solution. *J. Phys. Chem. B* **2002**, *106*, 2372–2380.

(26) Bensasson, R. V.; Bienvenue, E.; Dellinger, M.; Leach, S.; Seta, P. C_{60} in model biological systems - a Visible-Uv absorption study of solvent-dependent parameters and solute aggregation. *J. Phys. Chem.* **1994**, *98*, 3492–3500.
(27) Guldi, D. M.; Prato, M. Excited-state properties of C_{60} fullerene derivatives. *Acc. Chem. Res.* **2000**, *33*, 695–703.
(28) Nakajima, N.; Nishi, C.; Li, F. M.; Ikada, Y. Photo-induced cytotoxicity of water-soluble fullerene. *Fullerene Sci. Technol.* **1996**, *4*, 1–19.
(29) Tsuchiya, T.; Oguri, I.; Yamakoshi, Y. N.; Miyata, N. Novel harmful effects of [60]fullerene on mouse embryos in vitro and in vivo. *FEBS Lett.* **1996**, *393*, 139–145.
(30) Yang, X. L.; Fan, C. H.; Zhu, H. S. Photo-induced cytotoxicity of malonic acid [C_{60}]fullerene derivatives and its mechanism. *Toxicol. in Vitro* **2002**, *16*, 41–46.

ES702905G